Marine Hydrokinetic Energy from Western Boundary Currents

John M. Bane,[1] Ruoying He,[2] Michael Muglia,[3] Caroline F. Lowcher,[1,*] Yanlin Gong,[2] and Sara M. Haines[1]

[1]Department of Marine Sciences, University of North Carolina, Chapel Hill, North Carolina 27599-3300; email: bane@unc.edu, sarahaines@unc.edu

[2]Department of Marine, Earth, and Atmospheric Sciences, North Carolina State University, Raleigh, North Carolina 27695-8208; email: rhe@ncsu.edu, ygong3@ncsu.edu

[3]University of North Carolina Coastal Studies Institute, Wanchese, North Carolina 27891; email: muglia@csi.northcarolina.edu

Annu. Rev. Mar. Sci. 2017. 9:105–23

First published online as a Review in Advance on August 24, 2016

The *Annual Review of Marine Science* is online at marine.annualreviews.org

This article's doi: 10.1146/annurev-marine-010816-060423

*Present address: Scripps Institution of Oceanography, University of California, San Diego, La Jolla, California 92093; email: clowcher@ucsd.edu

Keywords

alternative energy, Gulf Stream, power density, Cape Hatteras, ocean turbine

Abstract

The kinetic energy in ocean currents, or marine hydrokinetic (MHK) energy, is a renewable energy resource that can help meet global energy requirements. An ocean circulation model–based census shows that subtropical surface western boundary currents (WBCs) are the only nearshore, large-scale currents swift enough to drive large electricity-generating ocean turbines envisioned for future use. We review several WBCs in the context of kinetic energy extraction. The power density in the Gulf Stream off North Carolina at times reaches several thousand watts per square meter at 75 m below the surface, and the annual average power is approximately 500–1,000 W m^{-2}. Significant fluctuations occur with periods of 3–20 days (Gulf Stream meanders) and weeks to months (Gulf Stream path shifts). Interannual variations in annual average power occur because of year-to-year changes in these WBC motions. No large-scale turbines presently exist, and the road to establishing MHK facilities in WBCs will encounter challenges that are similar in many aspects to those associated with the development of offshore wind power.

1. INTRODUCTION

The world's population climbed past 7 billion in 2011 and continues to rise. The rate of population increase, however, has been slowing since the 1960s, largely because many countries have been moving through the demographic transition. This rate decrease shows that the human population, although increasing in number, is not expanding exponentially (US Census Bureau 2016). By contrast, both energy usage and the rate of increase of energy usage continue to rise owing to the growing world population and the continued industrialization of developing countries, resulting in greater per capita energy use. Worldwide as well as domestically, approximately 85% of total energy production is from fossil fuels, approximately 10% is from renewable sources, and the remainder is from nuclear sources (EIA 2016). Because of continued concerns about the diminishing reserves of fossil fuels, increasing atmospheric CO_2 concentration, global warming, ocean acidification, and other effects from fossil fuel consumption, non-fossil-fuel sources are increasingly of interest—renewable sources in particular. The kinetic energy in moving ocean water, or marine hydrokinetic (MHK) energy, is one such renewable energy source. Surface waves, tidal currents, and large-scale currents contain most of the ocean's kinetic energy, and the current speeds of these motions are sufficiently high in many locations that some fraction of this energy could be extracted for electrical power production. MHK energy is currently being extracted from waves and tidal currents in certain locations throughout the oceans (e.g., Doran 2015), but commercial-size power plants have yet to be engineered and installed in any large-scale ocean currents (Neary et al. 2014a,b; BOEM 2016), even though the potential for generating electricity from the Gulf Stream in the Florida Straits has a long history of study (Stewart 1974, Von Arx et al. 1974, Lissaman & Radkey 1979, Lissaman 1980, Hanson et al. 2011).

In this article, we review MHK energy in the surface western boundary currents (WBCs) of the ocean's major subtropical gyres. These currents are persistent and swiftly flowing, with surface current speeds approaching and sometimes exceeding 3 m s^{-1}. WBCs have large cross-sectional areas—especially when compared with typical tidal current streams in inlets and estuaries, where some electricity-generating turbines are presently installed (Hogg & Johns 1995, Gunawan et al. 2014)—and flow along major portions of continental coastlines. These properties make WBCs desirable targets for alternative energy generation facilities. They are, with very few exceptions, the only large-scale oceanic currents with sufficiently high kinetic energy to reasonably consider MHK energy extraction with turbines. **Figure 1** shows a model calculation of all ocean currents with flow speeds fast enough at the 50-m depth level to give a three-year average kinetic energy flux (equivalent to power density) greater than 500 W m^{-2} (0.5 kW m^{-2}) (VanZwieten et al. 2013a). It is apparent that WBCs show average power densities above this level, but perhaps the more important fact shown by this figure is that, other than WBCs, almost the entire global ocean has power-density levels below this. For the purpose of extracting (a.k.a. harvesting, harnessing, or capturing) kinetic energy from ocean currents, it is fortuitous that many high-power-density regions are WBCs flowing close to shorelines.

Our purpose in this review is to describe the present understanding of the flow properties and power-density levels in WBCs in the context of harnessing a portion of that energy for electricity generation. As is typical of large-facility construction and operation in the marine environment, there are important engineering, environmental, legal, financial, and other-use considerations, which we do not discuss in detail here (see, e.g., Boehlert & Gill 2010, Neary et al. 2014b, Brown et al. 2015).

Section 2 describes MHK energy fundamentals, and Section 3 provides an overview of WBCs and their properties that are pertinent to energy extraction. Section 4 describes MHK details in the Gulf Stream off Cape Hatteras, North Carolina, United States. This location has been well

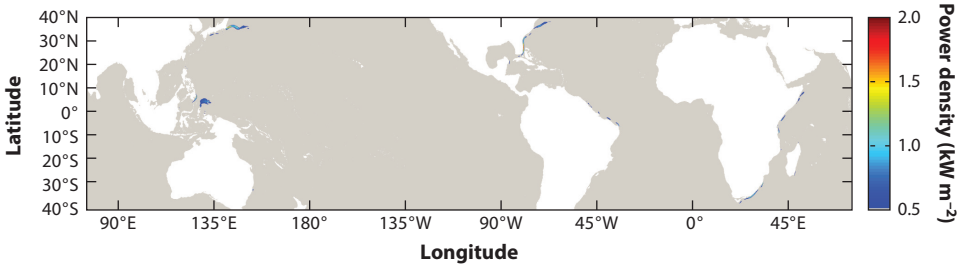

Figure 1

Areas with current speeds high enough to produce time-averaged power densities greater than 500 W m^{-2} (0.5 kW m^{-2}) at a depth of 50 m, as computed by the Hybrid Coordinate Ocean Model (HYCOM) for 2009–2011. Almost every colored area is a western boundary current. Depths less than 75 m are shown in white. Figure adapted from VanZwieten et al. (2013a). The ocean current data for the map came from the HYCOM global circulation model; for a description of HYCOM, see Chassignet et al. (2007).

studied, the Gulf Stream there has many properties that will affect MHK energy extraction and that are found in other WBCs, and the region has characteristics suitable for possible commercial development of electrical power generation at some future time (Kabir et al. 2015, Lowcher 2015, VanZwieten et al. 2015). Section 5 looks ahead to the future.

2. FUNDAMENTALS OF MARINE HYDROKINETIC ENERGY

Important aspects to evaluate when considering the extraction of MHK energy from a WBC include the current's power density; the spatial structure and temporal variability of the current; and the proximity of the current to land, population centers, and connections to the onshore power grid. Important engineering considerations include the type of turbine, mooring, and anchoring system to be used; the total water depth and bottom type where turbines will be installed; current variations with depth; and turbulence levels within the water column (Neary et al. 2014b, VanZwieten et al. 2015). Knowledge of these subjects has been increasing for several WBCs; however, as of the date of this article, large-scale electrical generation turbines suitable for deployment in a WBC are still in the development and prototype stages and have yet to be manufactured and commercially installed (Neary et al. 2014b, Ecomerit Technol. 2016, Southeast Natl. Mar. Renew. Energy Cent. 2016).

2.1. In-Stream Power

Extracting energy from a WBC with a turbine is a type of in-stream electrical power generation. In-stream means that the current in which the turbine is placed has not been impounded, as would be the case, for example, for water held behind a dam (VanZwieten et al. 2014a). Thus, the energy source in the current is only the kinetic energy in the current's flow. The current's kinetic energy flux is the amount of kinetic energy passing through a unit area that is oriented perpendicular to the current flow direction during a unit of time. This is equivalent to the current's power per unit area, or power density, P (typically expressed in watts per square meter), and is given by

$$P = \frac{1}{2}\rho S^3, \tag{1}$$

where S is the current speed normal to and through the unit area and ρ is the density of the water. To determine the total power in a WBC, P is integrated over the entire cross-sectional area

perpendicular to the current direction. Similarly, the power in the current flowing through any specific area, A, can be determined by integrating P over that area. If S is nearly uniform across A (which might be the case, for example, for the swept area of a turbine's blades), then the power over that area is

$$\text{power} = \frac{1}{2}\rho S^3 A = PA. \tag{2}$$

Many power resource assessments in ocean currents (as well as in the lower atmosphere for wind energy facilities) use observations, numerical model simulations, or both to determine the current (or wind) speed, S, from which the power density, P, is calculated for a location that appears suitable for generator installation.

2.2. Extracting Marine Hydrokinetic Energy

Several types of MHK energy extraction devices have been considered for ocean currents (e.g., Batten et al. 2006, Bedard 2008, Neary et al. 2014b, **http://www.marineturbines.com**). Here, we consider axial-flow (horizontal-axis) turbines (bladed-rotor generators). This type of device is similar to a submarine version of a typical wind turbine and is a larger-scale version of many marine turbines presently being used in tidal channels (e.g., Corren et al. 2013, **http://www.verdantpower.com**). The swept area of the turbine's rotor blades is called the blade circle.

The amount of MHK energy extracted from an ocean current by this type of turbine is less than the total kinetic energy in the current that flows through a turbine blade circle. That is, the extracted power divided by the blade-circle area is less than P for the current at the turbine location. This is a basic principle that is easy to visualize: The complete extraction of kinetic energy from the flow would reduce the current speed to zero, thus leaving motionless water on the downstream side of the blade circle, which would prevent further flow through the turbine. The theoretical maximum fraction of kinetic energy flowing through a blade circle that can be extracted by the rotor is 59%—the well-known Lanchester-Betz limit, commonly referred to as the Betz limit (Lanchester 1915, Betz 1920, Van Kuik 2007). A real turbine will extract an even smaller fraction than this because of friction, turbulence, wake generation, possible cavitation, vibration of the rotor/generator assembly, and so on. Two additional engineering constraints on real turbines are (*a*) that a turbine will not begin to rotate until the current reaches a speed sufficient to overcome the friction and inertia of the turbine and generator machinery (the start-up speed or cut-in speed, S_{START}) and (*b*) that a turbine will reach a maximum safe-rotation rate at some current speed (the maximum-rotation-rate current speed, S_{Rmax}) and will maintain that rotation rate even if the current speed continues to increase past S_{Rmax}. Thus, there will be no further increase in energy capture if the current speed exceeds S_{Rmax}.

Neary et al. (2014b) described a numerical model of a turbine rotor with an S_{START} of 0.5 m s^{-1} and an S_{Rmax} of 1.7 m s^{-1}. With a blade-circle diameter of 33 m and an assumed rotor power coefficient, C_p (the ratio between the power extracted by the rotor blades and the current's MHK power), of 0.48, a current speed of 1.7 m s^{-1} produces a maximum power extraction from the current of 1 MW (**Figure 2**). Published estimates of in-stream rotor power coefficients range from 0.3 (e.g., Gorban et al. 2001, Guney 2011) to approximately 0.5 (e.g., VanZwieten et al. 2013b, Neary et al. 2014b).

All of the extracted power will not be converted into electrical output from the turbine (rotor/generator system), however, owing to mechanical losses in the drive train (e.g., gearbox and bearings) that connects the rotor blades to the generator (~5%), electrical and mechanical losses in the generator (~10%), and losses within the power conditioning equipment that connects

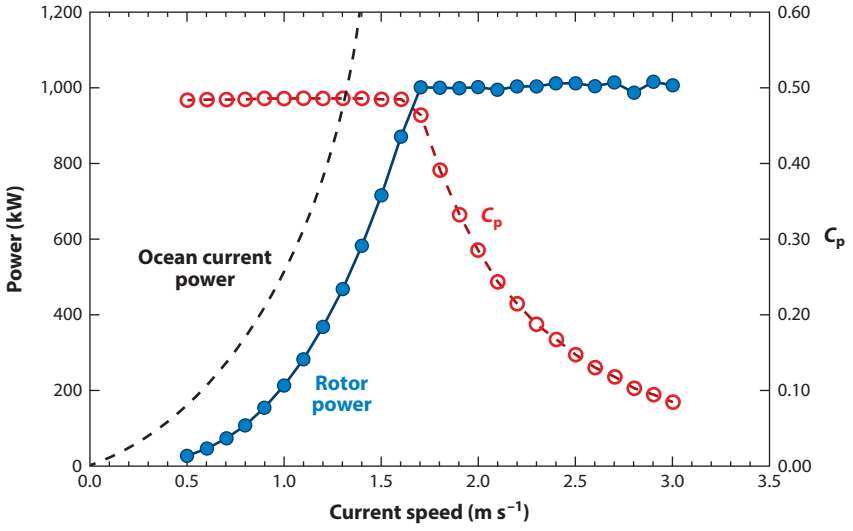

Figure 2

Ocean current power (*dashed black line*); rotor power (*solid blue line*); and rotor power coefficient, C_p (*dashed red line*), versus current speed for a 33-m-diameter, three-blade model rotor. The start-up current speed, S_{START}, is 0.5 m s^{-1}; the maximum-rotation-rate speed, S_{Rmax}, is 1.7 m s^{-1}; and the maximum rotor power coefficient is 0.48. Figure adapted from Neary et al. (2014b).

the generator to the cabling reaching to the onshore power grid (~10%). These estimated loss percentages were reported by Hagerman et al. (2006), who studied in-stream power extraction from a tidal current. Taking the rotor C_p to be 0.48, and assuming these losses to be reasonable for open-ocean in-stream power generation, we find that the delivered electrical power will be approximately 37% of the current's P times the turbine swept area (blade-circle area) for current speeds between S_{START} and S_{Rmax}. As a comparison, this value is approximately 45% for some popular wind turbines (e.g., from Vestas; see **http://www.vestas.com/en/products/turbines**). In Section 4, we present observed and modeled current speeds, power densities, and electrical power output potential for the Gulf Stream offshore of North Carolina.

3. WESTERN BOUNDARY CURRENTS

3.1. Jetlike Flow in Western Boundary Currents

Figure 3 is a schematic of the Gulf Stream as it flows poleward along the upper continental slope of the southeastern United States. The surface current maximum and the lateral and vertical shears in the jetlike horizontal velocity are evident. Each WBC in an oceanic subtropical gyre has a similar jetlike velocity structure as it flows along its continental boundary. Each WBC is approximately 100 km in width (80–150 km is the typical range) and 1,000 m in vertical extent (typical distance from the sea surface to the 0.2 m s^{-1} isotach), and each transports approximately 30–100 sverdrups (Sv) of seawater (1 Sv $= 10^6$ m^3 s^{-1}) (Imawaki et al. 2013). The downstream current speed is strongest at the surface near the center of the current (the surface-speed maximum is usually located somewhat to the shoreward side of the geometric center of the current jet), and the speed decreases in any direction away from the surface maximum. The typical maximum speed differs from one WBC to another, as shown in **Figure 4**. The differences among these WBC jets

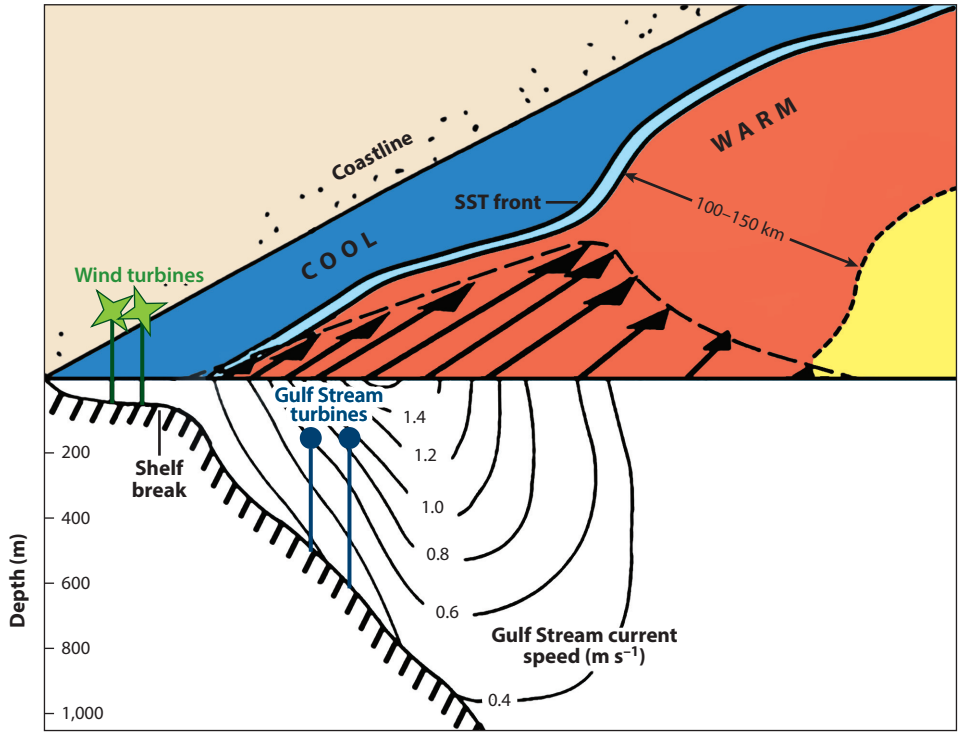

Figure 3

Schematic of the Gulf Stream's velocity structure along the southeastern United States. The inshore edge of the Gulf Stream, identifiable as the sea surface temperature (SST) front, meanders along the continental shelf break, located approximately 30–100 km offshore. The warm, jetlike current is fastest at the surface, and speeds diminish in all directions away from the surface maximum. The current's width is approximately 100 km, and its vertical extent is approximately 1,000 m. Most subtropical western boundary currents have a similar jetlike velocity structure, although the width and maximum speed may differ from one current to another (see **Figure 4**). For reference, the schematic also shows a typical location for offshore wind turbines (*green stars*), in shallow water on the continental shelf. Currents are much slower there than in the Gulf Stream, where subsurface ocean current turbines (*blue circles*) might be moored.

are apparent in the figure, including differences in current width (approximately 80 km for the Gulf Stream in the Florida Straits to more than 150 km for the Kuroshio off Japan and the Gulf Stream off Cape Hatteras) and maximum current speed (the Agulhas Current is strongest, at 1.7 m s^{-1}; the Brazil Coastal Current is weakest, at just under 0.6 m s^{-1}; and each of the other currents has a maximum speed of approximately 1.5 m s^{-1}).

3.2. Western Boundary Current Variability

WBCs are not steady currents. Each varies over a wide range of timescales, and any variations that give rise to current-speed fluctuations at a moored turbine site will affect power generation. Because of the narrow jet structure of WBCs (**Figures 1**, **3**, and **4**), lateral movements of the jet of a few kilometers to a few tens of kilometers can change the current speed at a fixed location by a large fraction of the current's maximum speed. In the extreme, a WBC will occasionally move laterally away from a fixed turbine location entirely, which means that no power will be generated until the current moves back and again flows through the turbine.

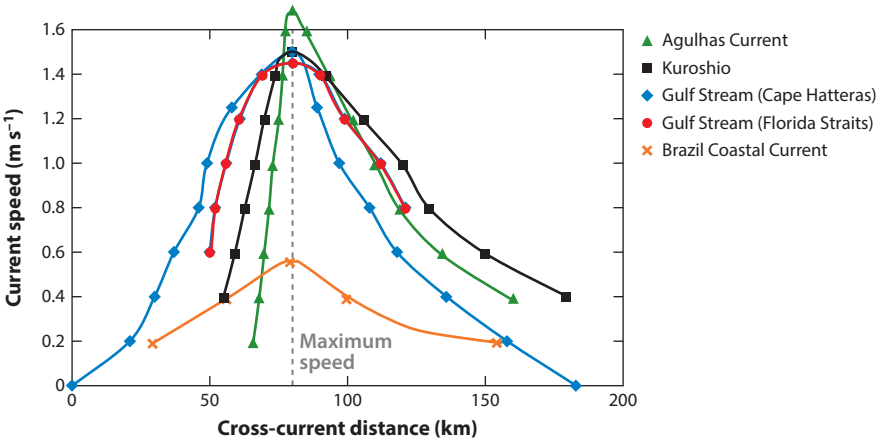

Figure 4

Cross-current profiles of downstream current speed at a depth of 75 m in four western boundary currents. Each profile is a synoptic instantaneous snapshot (as opposed to a long-term average) and has its speed maximum positioned at 80 km on the horizontal axis to more clearly show the similarity in the jetlike profiles. The depth of 75 m was chosen because this is a desirable depth at which to moor turbines. Note that there are two locations within the Gulf Stream: one off of southeastern Florida within the Florida Straits, and one off of Cape Hatteras. Data are from Bryden et al. (2005) (Agulhas Current), Zhu et al. (2001) (Kuroshio), Halkin & Rossby (1985) (Gulf Stream, Cape Hatteras), Leaman et al. (1987) (Gulf Stream, Florida Straits), and Johns et al. 1998 (Brazil Coastal Current).

Two common types of lateral WBC motions are propagating, wavelike meanders of the path of the current and lateral path shifts (Hogg & Johns 1995, Lee & Cornillon 1995, Imawaki et al. 2013). WBC meanders typically have periods of a few days to a few weeks, and path shifts can move a long stretch of the current laterally to a new position, where it may remain for weeks to months. In the Gulf Stream, meanders (e.g., Webster 1961, Lee 1975, Bane et al. 1981; see **Figure 7** in Section 4, below) and path shifts (e.g., Brooks & Bane 1981, Bane & Dewar 1988, Quattrocchi et al. 2012, Zeng & He 2016) have a long history of study. Such variations have been repeatedly observed in the Gulf Stream offshore of Cape Hatteras (Tracey & Watts 1986, Savidge 2004), and they have important impacts on the *P* levels in that region, as detailed in Section 4.

3.3. Energy Extraction from Western Boundary Currents

It will be desirable to position turbines as close to a WBC's high-speed core as possible while also being close enough to shore for electrical connection purposes and in water shallow enough for mooring. Turbines will likely need to be moored so that all components (in particular turbine blades) are sufficiently far below the surface wave zone and surface shipping traffic. **Figure 3** indicates positions within the water column where turbines might be moored. The pertinent depth level at which to consider *P* values is the subsurface hub depth, where the center of a turbine blade will reside. **Figure 5** shows maps of multiyear average power densities in four of the WBCs shown in **Figure 1**. In the study from which these two figures were adapted, VanZwieten et al. (2013a) chose 50 m as the hub depth for their study, so the *P* values in **Figures 1** and **5** will likely be slightly greater than those at 75 m (see Section 4 for a description of 75-m *P* values, both instantaneous and long-term averages, in the Gulf Stream). In a related article, VanZwieten et al. (2014b) compared the power levels computed from Hybrid Coordinate Ocean Model (HYCOM)

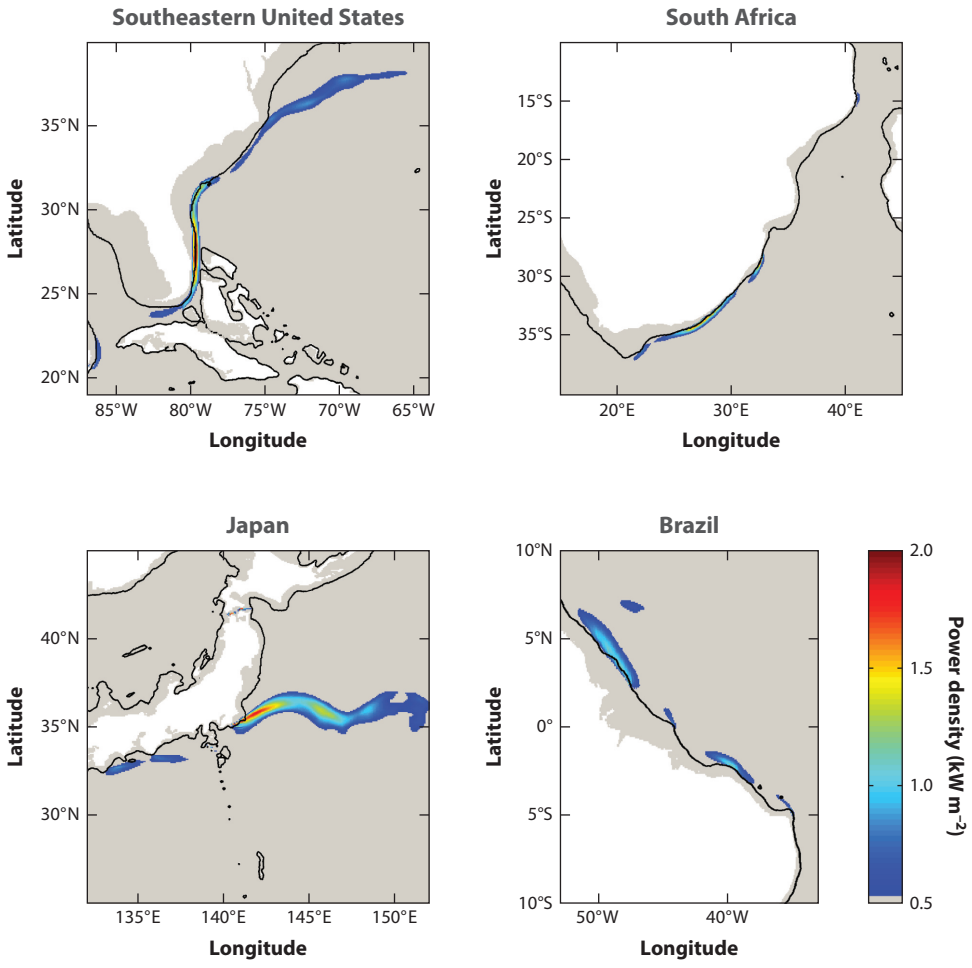

Figure 5

Four western boundary currents with current speeds high enough to produce time-averaged power densities greater than 500 W m^{-2} (0.5 kW m^{-2}) at a depth of 50 m, as computed by the Hybrid Coordinate Ocean Model (HYCOM) for 2009–2011. The black lines are 500-m isobaths. **Figure 4** shows the cross-current profiles of downstream speeds in these currents. Figure adapted from VanZwieten et al. (2013a).

model speeds with those observed in the Florida Straits and in the Agulhas Current and found that the HYCOM values can differ from the observed values by 8% to approximately 40%. Their study highlights one of the challenges in power resource estimates in ocean currents. The computation of *P*, from either measured or modeled current speed, *S*, almost always uses Equation 1, and because *P* is directly proportional to the cube of *S*, small differences between modeled and observed speeds can translate to large differences in *P*. Thus, a model that has good skill in simulating currents at a potential turbine site might not have a similar skill in providing an assessment of power density. In some cases, it is even possible for model simulations to have an annual average *S* that is somewhat higher (lower) than that observed, while the model's annual average *P* is computed to be lower (higher) than observed because of a mismatch in the observed and modeled temporal variability of *P*. Section 4 presents an example of the former.

The narrowness of the high-*P* regions within WBCs is apparent in **Figures 1** and **5**, consistent with the small cross-stream scale of a WBC jet (~100 km) when compared with its downstream length (thousands of kilometers). Although the jet structure of a WBC can remain roughly the same along much of its course, the lateral meandering and shifting of the jet can vary greatly from one segment of the current to another. The more that a narrow jet moves laterally, the wider and more smeared out the average speed and power-density patterns will be, resulting in lower maximum average *P* levels. Where lateral movements are less, there will tend to be higher *P* levels, especially near the high-speed core of the current. This pattern is apparent in the Gulf Stream in **Figure 5**, where the higher-*P* regions are in the segments of the Gulf Stream where meanders have lower lateral amplitudes—within and somewhat north of the Florida Straits and offshore of Cape Hatteras (Miller 1994). This pattern is described further in the next section (see **Figure 11** in Section 4.1, below).

4. MARINE HYDROKINETIC ENERGY FROM THE GULF STREAM ALONG NORTH CAROLINA

Here we describe the Gulf Stream in the South Atlantic Bight, which is the region of the Atlantic Ocean over the continental shelf and slope extending from the northern Florida Straits to Cape Hatteras. We discuss MHK power characteristics throughout the South Atlantic Bight, focusing on a region off the coast of North Carolina where the continental shelf is narrow, the Gulf Stream's lateral position variability is lowest for the entire east coast after it leaves the Florida Straits, and the Gulf Stream flows with its shoreward edge relatively close to the shoreline as it passes Cape Hatteras (**Figure 6**). Utilizing observations from a bottom-moored, 150-kHz acoustic Doppler current profiler (ADCP) and numerical results from a regional ocean circulation model [the Regional Ocean Modeling System (ROMS) model (Shchepetkin & McWilliams 2005) embedded within the global HYCOM model (Gong et al. 2015)], we describe the current-speed and power-density values within the Gulf Stream east of Cape Hatteras. Comparisons between observed and modeled power densities indicate the skill of the model at the ADCP location during 2014. Within this skill level (details provided below), the model may be used for power resource assessments at nearby locations and at other times, where and when observations are not available. **Figure 7** shows a close-up of the area of interest along the North Carolina coast, which extends from approximately 32.5°N to 35°N and from 74°W to 77°W, along with the 2014 vector-average velocities at a depth of 75 m at each station along three cross-isobath transects.

4.1. Gulf Stream Meanders and Path Shifts Have Major Effects on Power Density

Figure 8 shows the current speed at a depth of 75 m as measured by the ADCP and computed by the ROMS model at the ADCP site for 2014. The ADCP annual average speed is 1.04 m s^{-1}, which is very close to the model's annual average speed of 1.07 m s^{-1}. Although these averages are quite close to one another, it is apparent that the speed fluctuations in the two time series have periods of several days (resulting primarily from Gulf Stream meanders) that are often not in phase and are generally of differing amplitudes. Important to keep in mind in this regard is that the ADCP measurements and the model calculations are independent of one another—that is, the ADCP data were not assimilated in this model hindcast for 2014.

More slowly varying fluctuations, with periods of approximately three weeks or longer, also occurred in the speed time series. These are due to large-along-stream-scale, lateral shifts in the Gulf Stream's path. At times, these shifts moved the Gulf Stream sufficiently offshore that

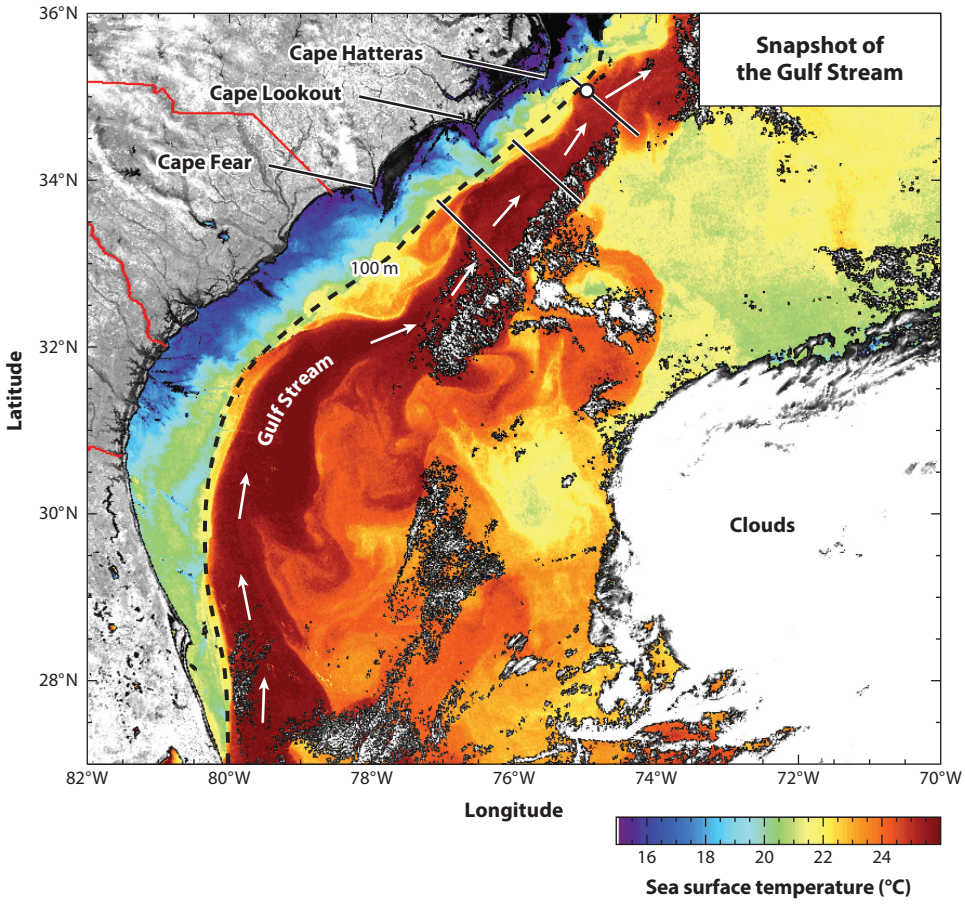

Figure 6

A sea surface temperature (SST) snapshot of the Gulf Stream flowing through the South Atlantic Bight in March 2008. Raleigh Bay is located between Cape Hatteras and Cape Lookout, and Onslow Bay is between Cape Lookout and Cape Fear. The three cross-isobath transects shown in **Figure 7** are represented here by the northwest-southeast-oriented solid black lines. Note that the Gulf Stream is closest to the coast off of Cape Hatteras and in the Florida Straits (just south of the lower picture border), where the continental shelf (the coastline to the 100-m isobath) is narrowest. The meandering path of the Gulf Stream is apparent in this image. The white dot near the shoreward end of the northeasternmost transect is the location of the moored acoustic Doppler current profiler (ADCP) that provided the data for subsequent figures.

the power at the ADCP site during these path-shifted episodes was relatively low. Four periods of lower speeds measured by the ADCP become apparent when the shorter-period, meander fluctuations are filtered out of the time series. **Figure 9** shows the 21-day low-pass-filtered ADCP speed time series, and the four offshore path shifts are identifiable when current speeds were low: March, June, late September to mid-October, and late November to mid-December.

Power densities at a depth of 75 m at the ADCP site, computed using the ADCP-measured current speed and the ROMS model current speed, are plotted together in **Figure 10**. Variations in each of the time series can be seen at meander periodicities and at path-shift timescales. The four periods of lower speed in **Figure 9** are also indicated in this figure, showing that the lower speeds during path-shifted periods resulted in much lower *P* levels at the ADCP site. The 2014

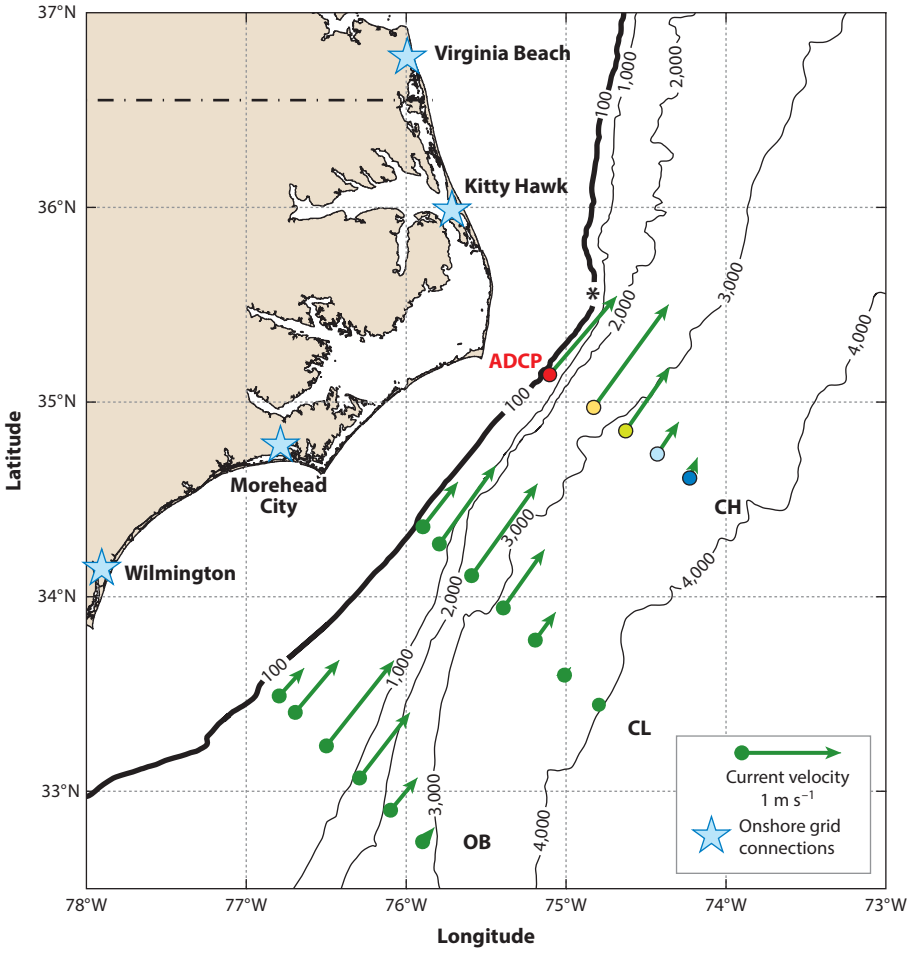

Figure 7

Average current velocities at a depth of 75 m for the three cross-isobath transects shown in **Figure 6** [Cape Hatteras (CH), Cape Lookout (CL), and Onslow Bay (OB)], as computed by the Regional Ocean Modeling System (ROMS) model for 2014. Colored dots indicate the locations of stations along these transects; the different colors along the CH transect identify the five stations for which **Figure 12** provides power-density data, below. The black contour lines are isobaths (in meters), with the 100-m isobath (approximately the shelf break) shown in bold. Each transect extends across most of the Gulf Stream's Eulerian-average jet, as shown by the green arrows. The narrower, cyclonic-shear side of the Gulf Stream jet (shoreward side) and the wider, anticyclonic-shear side of the jet (seaward side) are clear in this average velocity distribution. The moored acoustic Doppler current profiler (ADCP) is located at the red dot on the Cape Hatteras transect, and this is also a model station. The ADCP site was chosen to be approximately centrally located within the cyclonic-shear side of the Gulf Stream at a depth of approximately 225 m, and it is in a region where the lateral meandering of the Gulf Stream is relatively small. It is also close to the shoreline and is approximately the same distance from two onshore grid connection sites (Morehead City and Kitty Hawk). Both the model and ADCP-observed velocity vectors are plotted at the red dot, and they are similar enough to overlie one another. The asterisk on the 100-m isobath to the northeast of the ADCP denotes "The Point," which is the northern extent of the South Atlantic Bight, where the continental shelf makes an abrupt change in orientation. The four blue stars show the locations of cities where connections can be made to the onshore electrical power grid.

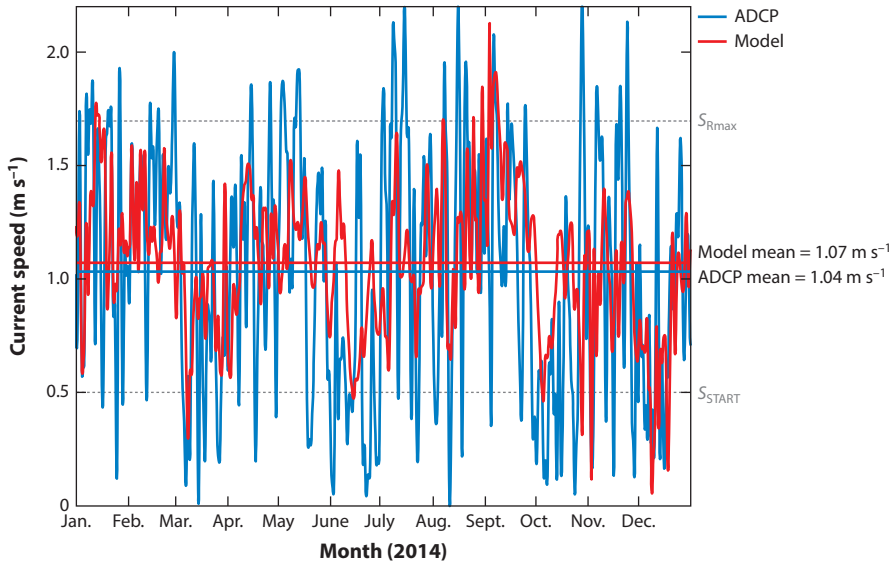

Figure 8

Time series of the current speed at a depth of 75 m at the moored acoustic Doppler current profiler (ADCP) site in 2014. The ADCP-measured speed is shown in blue, and the Regional Ocean Modeling System (ROMS) model speed is shown in red. The blue horizontal line shows the ADCP average speed (1.04 m s^{-1}), and the red horizontal line shows the model average speed (1.07 m s^{-1}). The lower dashed line indicates a rotor start-up speed, S_{START}, of 0.5 m s^{-1}, below which the turbine described in **Figure 2** would produce no power. The upper dashed line indicates the maximum-rotation-rate current speed, S_{Rmax}, of 1.7 m s^{-1} for that turbine, above which the power generated would no longer increase.

annual average P from the ADCP is 1,000 W m^{-2}, whereas that from the model is 790 W m^{-2}, 21% less than the ADCP average. This is interesting in that the model's average speed is 3% greater than the ADCP's average speed. The P averages are reversed in relative magnitude from the speed magnitudes because of the larger-amplitude speed variations measured by the ADCP compared with those computed by the model. When speed is cubed to calculate P (Equation 1), the greater peak ADCP speed values, mostly during passing Gulf Stream meanders, produce greater power densities than do the model speeds.

Figure 11 plots the power density at 75 m along the Gulf Stream throughout the South Atlantic Bight and to approximately 500 km northeast of Cape Hatteras as computed by the ROMS model. The annual average model power density at the moored ADCP site was computed to be 790 W m^{-2} (**Figure 10**). As described in Section 3.3, the variation in P along the Gulf Stream is due mainly to the amount of lateral movement of the jet. Just south of the lower border of the region shown in **Figure 11**, meanders are confined laterally within the Florida Straits by the shallow Bahama Banks on the eastern side of the straits and the presence of the Florida peninsula along the western side. As the Gulf Stream flows northward out of the Florida Straits, meanders grow in lateral amplitude as they propagate poleward with phase speeds of approximately 20–60 km day^{-1} (Lee et al. 1981, Bane & Dewar 1988). This growth continues until the meanders reach approximately 32°N, which is where the path of the Gulf Stream is deflected toward the east by a bottom topographic rise, the Charleston Bump (Brooks & Bane 1978, Legeckis 1979). The downstream growth in lateral meandering along this portion of the Gulf Stream results in the downstream decrease in average P apparent in **Figure 11*a***, from where the Gulf Stream exits the Florida Straits to approximately

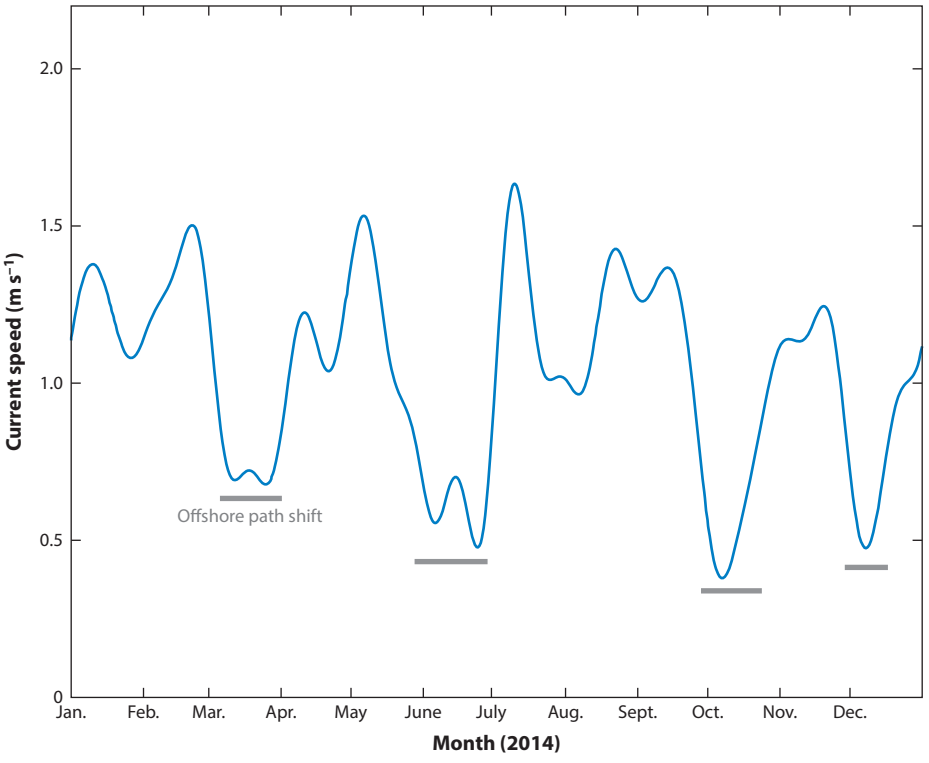

Figure 9

Current-speed time series from the moored acoustic Doppler current profiler (ADCP). A 21-day low-pass filter was applied to the ADCP-measured speed shown in **Figure 8** to remove fluctuations with periods of three weeks or less, which are due mostly to Gulf Stream meanders. Four offshore path shifts of the Gulf Stream occurred during 2014, and the current speed was generally lower during each of these episodes. These shifts are visible in March, June, late September to mid-October, and late November to mid-December (*gray horizontal bars*).

31.5°N, where it begins to turn seaward as it enters the deflection region. Meander amplitudes grow rapidly from 32°N to approximately 33.5°N because the Gulf Stream is destabilized by flowing over the Charleston Bump (Gula et al. 2015), and the further decrease in average P in this stretch of the current is visible in **Figure 11**. The restabilizing effect of the increasing bottom slope between 33.5°N and "The Point" (see **Figure 7**) results in decreasing meander amplitudes and an attendant increase in average P there.

The annual average P distribution in **Figure 11** highlights how important careful positioning of a turbine or turbine array is, owing to the narrowness of the high-power-density region in the Gulf Stream. This is typical of all WBCs. A turbine placed only a few kilometers to a few tens of kilometers away from another could make a difference of several hundred watts per square meter of available power density. Both careful analyses of previous current data and good forecasts for future WBC positions are needed to guide turbine facility emplacements.

4.2. Interannual Variations in Power

The variability in any WBC, like that within the Gulf Stream described above, is different in detail from one year to another, and this will likely produce year-to-year differences in the annual

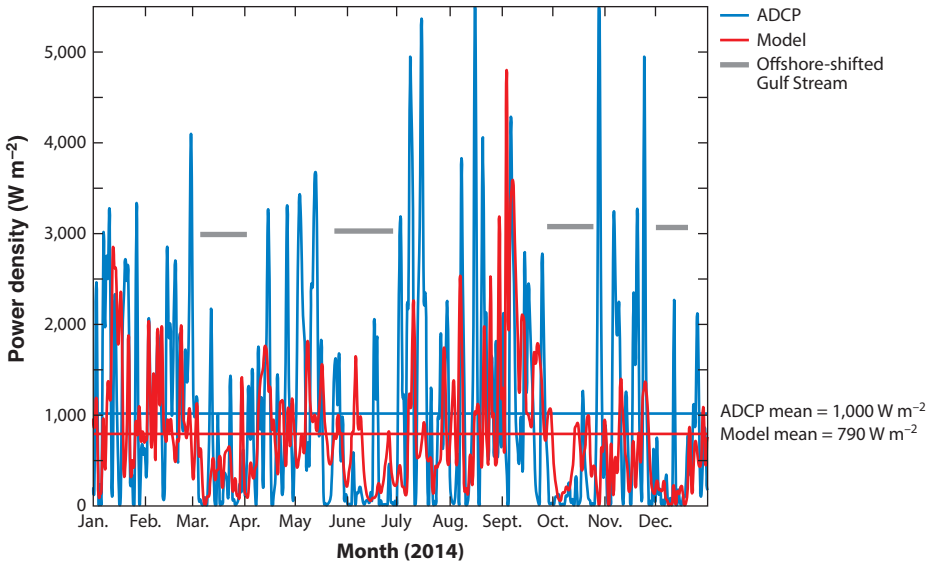

Figure 10

Time series of power density, *P*, at a depth of 75 m at the moored acoustic Doppler current profiler (ADCP) site for 2014, computed from moored ADCP speed data and the Regional Ocean Modeling System (ROMS) model. The moored ADCP *P* is shown in blue, and the model *P* is shown in red. The blue horizontal line shows the ADCP's annual average power density of 1,000 W m^{-2}, and the red horizontal line shows the model's annual average power density of 790 W m^{-2}. The four episodes of offshore-shifted Gulf Stream shown in **Figure 9** are again indicated by gray horizontal bars.

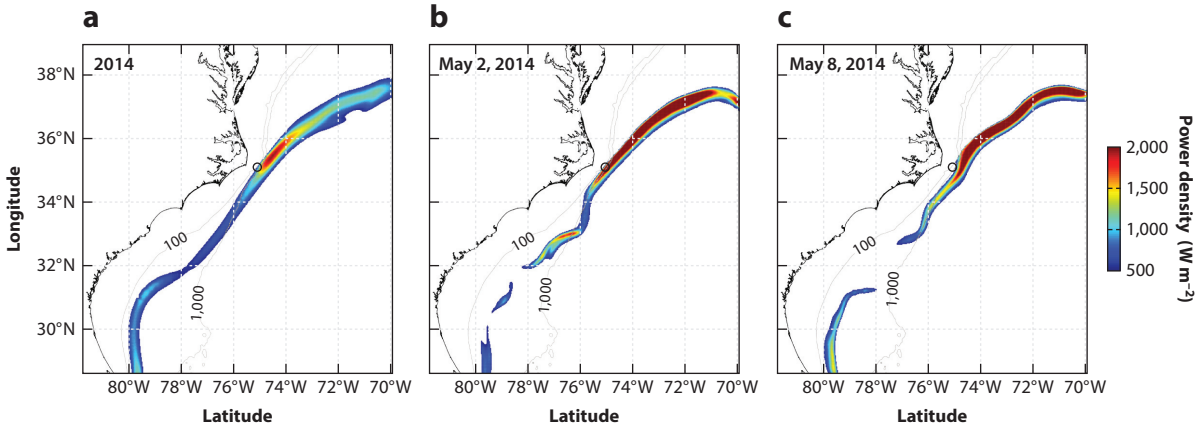

Figure 11

Power density, *P*, at a depth of 75 m throughout the South Atlantic Bight, as computed by the Regional Ocean Modeling System (ROMS): (*a*) the 2014 annual average; (*b*) the daily average for May 2, 2014; and (*c*) the daily average for May 8, 2014. The open circle in each panel shows the location of the moored acoustic Doppler current profiler (ADCP) site. The along-stream variation in annual average *P* is apparent, as is the average value of 790 W m^{-2} at the ADCP site. A meander pattern in the Gulf Stream propagated northeastward between May 2 and May 8, and the model power density at the site decreased from almost 2,000 W m^{-2} to less than 500 W m^{-2}, as shown in **Figure 9**.

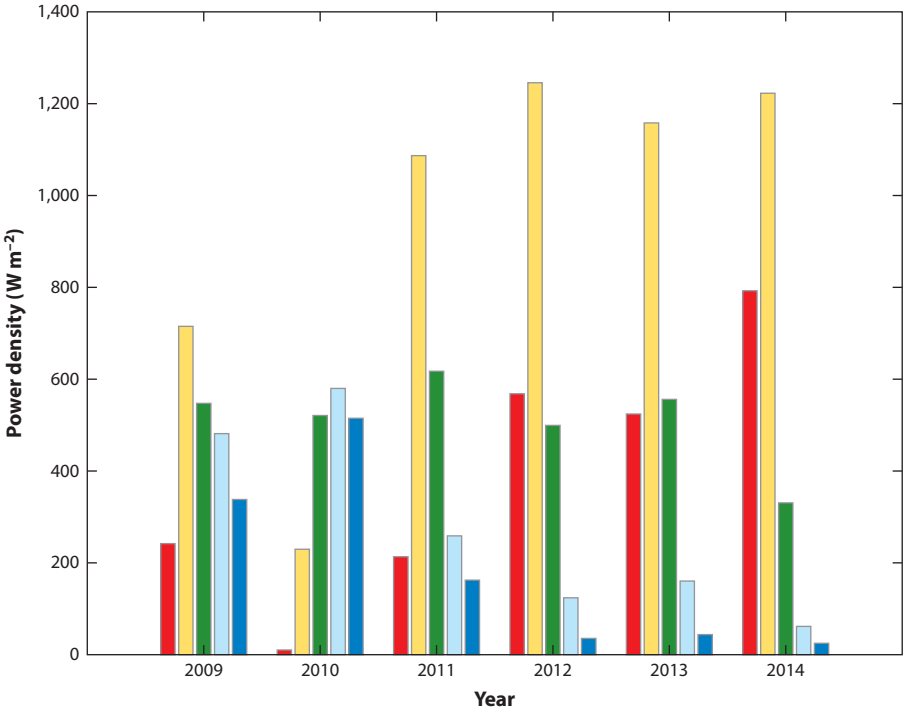

Figure 12

Annual average model power density, *P*, at a depth of 75 m at each station on the Cape Hatteras (CH) transect for 2009–2014. The locations of the five stations are shown on the CH transect in **Figure 7**, and the bar colors here correspond to the station colors shown in that figure. For each year, the bars are ordered from the most shoreward station [the moored acoustic Doppler current profiler (ADCP) site; *red*] to the most seaward station (*blue*).

average power density at a fixed site. To assess the interannual power variations on the Cape Hatteras transect (labeled CH in **Figure 7**), we have used ROMS hindcast current speeds to compute annual average power density at 75 m at each station on this transect for 2009 through 2014. **Figure 12** shows the average *P* values for each year and station. In each year (with the exception of 2011), the *P* levels varied along the transect in a manner similar to the Gulf Stream's jetlike velocity profile. The amount of meandering and shifting is usually such that the Gulf Stream's jetlike character is reflected in the power-density pattern—highest at one station in the central portion of the distribution and tapering off to low on either side. During 2011, there was an almost uniform *P* distribution across four of the five stations, indicating a wider range of jet meandering and/or shifting.

Clear year-to-year variations in *P* occur throughout this time period at each station on the Cape Hatteras transect. This is also the case for the two other transects in **Figure 7** (not shown in **Figure 12**; see Lowcher 2015). These variations include the station at which the highest *P* level occurred (the yellow station in each year except for 2010 and possibly 2011), the *P* value at the annual peak (from 380 W m^{-2} in 2011 to 1,250 W m^{-2} in 2012), and the total annual average *P* across the five stations (from 1,450 W m^{-2} in 2011 to 2,515 W m^{-2} in 2013). An interesting comparison can now be made with the power of the wind at a location over the middle of the

continental shelf off of Cape Hatteras, approximately 20 km shoreward from the ADCP site. Thomas et al. (2015) reported the multiyear average (2008–2012) of wind power density at a wind turbine hub height of 100 m above the sea surface to be 600–800 W m^{-2}, reasonably comparable to the ocean current power-density levels shown in **Figure 12**.

5. LOOKING AHEAD

A sometimes-heard phrase in environmental, natural resources, sociology, and economics courses is "energy equals human activity"—that is, per capita energy use rate correlates strongly with economic standard of living. Given the need to (literally) fuel the human population's growing energy requirements while also endeavoring to minimize adverse environmental effects, alternative energy sources are increasingly of interest. We have reviewed here the nature of oceanic WBCs in the context of harvesting kinetic energy from them, which could add to the ensemble of alternative energy sources in future years. A global census of current speeds in the oceans at a typical ocean turbine hub depth points to WBCs as the only large-scale currents flowing swiftly enough to drive the type of electricity-generating MHK turbines envisioned for use in coming decades. A fortuitous aspect of this is that a WBC flows along a continental coastline for a good fraction of its length, naturally close to shore and, in places, close to population centers.

The journey to establishing arrays of ocean turbines spinning in WBCs and sending gigawatts of electrical power to onshore populations will be a long one. Some lessons regarding the many steps involved—engineering the designs of turbines and array geometries, moving through permitting and leasing procedures with various governmental entities, performing environmental and other impact studies, making long cable connections to shore, and dealing with unsteady power production from such generation facilities, among others—have and will continue to come from recent offshore wind efforts. Even so, important differences between wind and ocean current power need to be appreciated. To this end, we mention the two urban legends of ocean current power (lead author's words): "Unlike the wind, the Gulf Stream is always flowing," and "ocean water is so much denser than air [800 times] that slower ocean currents have much more power than faster winds." We propose these new urban truths: "The Gulf Stream is always flowing, but it is not always in the same place," and "the greater density of ocean water as compared with air compensates for speed differences [$\sim$1 m s^{-1} for currents and $\sim$10 m s^{-1} for winds], resulting in comparable power densities for both currents and winds." Hopefully the first urban truth is apparent from this review. The second can be seen in these estimates (and in the comparison of ocean current power with wind power given at the end of Section 4):

$$P_{\mathrm{WIND}} \sim \frac{1}{2}(1.2\,\mathrm{kg\,m^{-3}})(10\,\mathrm{m\,s^{-1}})^3 \sim 600\,\mathrm{W\,m^{-2}},$$

$$P_{\mathrm{CURRENT}} \sim \frac{1}{2}(10^3\,\mathrm{kg\,m^{-3}})(1\,\mathrm{m\,s^{-1}})^3 \sim 500\,\mathrm{W\,m^{-2}}.$$

We hope this review, together with many other recent and informative ocean current energy studies, provides a realistic information base from which to progress.

DISCLOSURE STATEMENT

The authors are not aware of any affiliations, memberships, funding, or financial holdings that might be perceived as affecting the objectivity of this review.

ACKNOWLEDGMENTS

The authors have benefited from discussions with and suggestions from Joe DeCarolis, Billy Edge, Mo Gabr, Harvey Seim, Jim VanZwieten (who kindly provided **Figures 1** and **5**), Chris Garrett, and Russ Davis. We gratefully acknowledge the North Carolina Renewable Ocean Energy Program for supporting research into the MHK potential off North Carolina.

LITERATURE CITED

Bane JM, Brooks DA, Lorenson KR. 1981. Synoptic observations of the three-dimensional structure and propagation of Gulf Stream meanders along the Carolina continental margin. *J. Geophys. Res.* 86:6411–25

Bane JM, Dewar WK. 1988. Gulf Stream bimodality and variability downstream of the Charleston Bump. *J. Geophys. Res.* 93:6695–710

Batten WMJ, Bahaj AS, Molland AF, Chaplin JR. 2006. Hydrodynamics of marine current turbines. *Renew. Energy* 31:249–56

Bedard R. 2008. *Prioritized research, development, deployment and demonstration (RDD & D) needs: marine and other hydrokinetic renewable energy*. Rep., Electric Power Res. Inst., Palo Alto, CA

Betz A. 1920. Das Maximum der theoretisch möglichen Ausnützung des Windes durch Windmotoren. *Z. Gesamte Turbinenwesen* 26:307–9

Boehlert GW, Gill AB. 2010. Environmental and ecological effects of ocean renewable energy development: a current synthesis. *Oceanography* 23(2):68–81

BOEM (Bur. Ocean Energy Manag.). 2016. *Ocean current energy*. **http://www.boem.gov/Renewable-Energy-Program/Renewable-Energy-Guide/Ocean-Current-Energy.aspx**

Brooks DA, Bane JM. 1978. Gulf Stream deflection by a bottom feature off Charleston, South Carolina. *Science* 201:1225–26

Brooks DA, Bane JM. 1981. Gulf Stream fluctuations and meanders over the Onslow Bay upper continental slope. *J. Phys. Oceanogr.* 11:247–56

Brown A, Beiter P, Heimiller D, Davidson C, Denholm P, et al. 2015. *Estimating renewable energy economic potential in the United States: methodology and initial results*. Tech. Rep. NREL/TP-6A20-64503, Natl. Renew. Energy Lab., Golden, CO

Bryden H, Beal LM, Duncan LM. 2005. Structure and transport of the Agulhas Current and its temporal variability. *J. Oceanogr.* 61:479–92

Chassignet EP, Hurlburt HE, Smedstad OM, Halliwell GR, Hogan PJ, et al. 2007. The HYCOM (Hybrid Coordinate Ocean Model) data assimilative system. *J. Mar. Syst.* 65:60–83

Corren D, Hughes S, Paquette J, Sotiropoulos F, Calkins J. 2013. *Improved structure and fabrication of large, high-power KHPS rotors*. Tech. Rep. DOE/GO18168, Verdant Power, New York, NY

Doran C. 2015. Power from the sea. *J. Homel. Def. Secur. Inf. Anal. Cent.* 2:3–6

Ecomerit Technol. 2016. *Aquantis*. **http://ecomerittech.com/aquantis.php**

EIA (Energy Inf. Admin.). 2016. *Frequently asked questions*. **http://www.eia.gov/tools/faqs**

Gong Y, He R, Gawarkiewicz GG, Savidge DK. 2015. Numerical investigation of coastal circulation dynamics near Cape Hatteras, North Carolina, in January 2005. *Ocean Dyn.* 65:1–15

Gorban AN, Gorlov AM, Silantyev VM. 2001. Limits of the turbine efficiency for free fluid flow. *J. Energy Resour. Technol.* 123:311–17

Gula J, Molemaker MJ, McWilliams JC. 2015. Gulf Stream dynamics along the southeastern U.S. seaboard. *J. Phys. Oceanogr.* 45:690–715

Gunawan B, Neary VS, Colby J. 2014. Tidal energy site resource assessment in the East River tidal strait, near Roosevelt Island, New York, New York. *Renew. Energy* 71:509–17

Guney MS. 2011. Evaluation and measures to increase performance coefficient of hydrokinetic turbines. *Renew. Sustain. Energy Rev.* 15:3669–75

Hagerman G, Polagye B, Bedard R, Previsic B. 2006. *Methodology for estimating tidal current energy resources and power production by tidal in-stream energy conversion (TISEC) devices*. Rep. EPRI-TP-001 NA Rev 2, Electr. Power Res. Inst., Palo Alto, CA

Halkin D, Rossby T. 1985. The structure and transport of the Gulf Stream at 73°W. *J. Phys. Oceanogr.* 15:1439–52

Hanson HP, Bozek A, Duerr A. 2011. The Florida current: a clean but challenging energy resource. *Eos Trans. AGU* 92:29–36

Hogg NG, Johns WE. 1995. Western boundary currents. *Rev. Geophys.* 33:1311–34

Imawaki S, Bower A, Beal L, Qiu B. 2013. Western boundary currents. In *Ocean Circulation and Climate: A 21st Century Perspective*, ed. G Siedler, SM Griffies, J Gould, JA Church, pp. 305–38. Oxford, UK: Academic. 2nd ed.

Johns WE, Lee TN, Beardsley RC, Candela J, Limeburner R, Castro B. 1998. Annual cycle and variability of the North Brazil Current. *J. Phys. Oceanogr.* 28:103–28

Kabir A, Lemongo-Tchamba I, Fernandez A. 2015. An assessment of available ocean current hydrokinetic energy near the North Carolina shore. *Renew. Energy* 80:301–7

Lanchester FW. 1915. A contribution to the theory of propulsion and the screw propeller. *Trans. Inst. Nav. Archit.* 57:98–116

Leaman KD, Molinari RL, Vertes PS. 1987. Structure and variability of the Florida Current at 27°N: April 1982–July 1984. *J. Phys. Oceanogr.* 17:565–83

Lee T, Cornillon P. 1995. Temporal variation of meandering intensity and domain-wide lateral oscillations of the Gulf Stream. *J. Geophys. Res.* 100:13603–613

Lee TN. 1975. Florida current spin-off eddies. *Deep-Sea Res. Oceanogr. Abstr.* 22:753–65

Lee TN, Atkinson LP, Legeckis R. 1981. Observations of a Gulf Stream frontal eddy on the Georgia continental shelf, April 1977. *Deep-Sea Res. A* 28:347–78

Legeckis RV. 1979. Satellite observations of the influence of bottom topography on the seaward deflection of the Gulf Stream off Charleston, South Carolina. *J. Phys. Oceanogr.* 9:483–97

Lissaman PBS. 1980. The Coriolis program. *Oceanus* 22:23–28

Lissaman PBS, Radkey RL. 1979. Coriolis program: a review of the status of the ocean turbine energy system. *Oceans* 79:559–65

Lowcher CF. 2015. *An assessment of marine hydrokinetic (MHK) energy in the Gulf Stream off Cape Hatteras*. BS Thesis, Univ. North Carolina, Chapel Hill

Miller JL. 1994. Fluctuations of Gulf Stream frontal position between Cape Hatteras and the Straits of Florida. *J. Geophys. Res.* 99:5057–64

Neary V, Lawson M, Previsic M, Copping A, Hallett KC, et al. 2014a. Methodology for design and economic analysis of marine energy conversion (MEC) technologies. In *Proceedings of the 2nd Marine Energy Technology Symposium, April 15–18, 2014, Seattle, WA.* **http://www.globalmarinerenewable.com/images/pdf/METS_PAPERS_VII/90-Neary.pdf**

Neary V, Previsic M, Jepsen RA, Lawson MJ, Yu Y-H, et al. 2014b. Reference model 4 (RM4): ocean current turbine. In *Methodology for Design and Economic Analysis of Marine Energy Conversion (MEC) Technologies*, ed. V Neary, M Previsic, RA Jepsen, MJ Lawson, Y-H Yu, et al., pp. 180–228. Albuquerque, NM: Sandia Natl. Lab.

Quattrocchi G, Pierini S, Dijkstra HA. 2012. Intrinsic low-frequency variability of the Gulf Stream. *Nonlinear Process. Geophys.* 19:155–64

Savidge DK. 2004. Gulf Stream meander propagation past Cape Hatteras. *J. Phys. Oceanogr.* 34:2073–85

Shchepetkin AF, McWilliams JC. 2005. The regional ocean modeling system (ROMS): a split-explicit, free-surface, topography-following-coordinate oceanic model. *Ocean Model.* 9:347–404

Southeast Natl. Mar. Renew. Energy Cent. 2016. *Technology testing.* **http://coet.fau.edu/focus-areas/technology-testing.html**

Stewart HB. 1974. Current from the current. *Oceanus* 17:38–41

Thomas N, Seim H, Haines S. 2015. An observational, spatially explicit, stability-based estimate of the wind resource off the shore of North Carolina. *J. Appl. Meteorol. Climatol.* 54:2407–25

Tracey KL, Watts DR. 1986. On Gulf Stream meander characteristics near Cape Hatteras. *J. Geophys. Res.* 91:7587–602

US Census Bureau. 2016. *Total midyear population for the world: 1950–2050*. **http://www.census.gov/population/international/data/worldpop/table_population.php**

Van Kuik GAM. 2007. The Lanchester-Betz-Joukowsky limit. *Wind Energy* 10:289–91

VanZwieten JH, Baxley WE, Alsenas GM, Meyer I, Muglia M, et al. 2015. Marine renewable energy—ocean current turbine mooring considerations. In *Proceedings of the Offshore Technology Conference*, *4–7 May*, *Houston*, *Texas*, Doc. OTC-25965-MS. Houstin, TX: Offshore Technol. Conf.

VanZwieten JH, Duerr AES, Alsenas GM, Hanson HP. 2013a. Global ocean current energy assessment: an initial look. In *Proceedings of the 1st Marine Energy Technology Symposium*, *April 10–11*, *Washington*, *DC*. **http://www.globalmarinerenewable.com/images/global%20ocean%20current%20energy%20assessment%20an%20initial%20look.pdf**

VanZwieten JH, McAnally W, Ahmad J, Davis T, Martin J, et al. 2014a. In-stream hydrokinetic power: review and appraisal. *J. Energy Eng.* 141:04014024

VanZwieten JH, Meyer I, Alsenas GM. 2014b. Evaluation of HYCOM as a tool for ocean current energy assessment. In *Proceedings of the 2nd Marine Energy Technology Symposium*, *April 15–18*, *Seattle*, *WA*. **http://www.globalmarinerenewable.com/images/pdf/METS_PAPERS_VII/100-VanZweiten.pdf**

VanZwieten JH, Vanrietvelde N, Hacker BL. 2013b. Numerical simulation of an experimental ocean current turbine. *IEEE J. Ocean. Eng.* 38:131–43

Von Arx WS, Stewart HB, Apel JR. 1974. The Florida Current as a potential source of usable energy. In *Proceedings of the MacArthur Workshop on the Feasibility of Extracting Usable Energy From the Florida Current*, ed. HB Stewart, pp. 91–101. Miami, FL: NOAA Atl. Oceanogr. Meteorol. Lab.

Webster F. 1961. A description of Gulf Stream meanders off Onslow Bay. *Deep-Sea Res.* 9:130–43

Zeng X, He R. 2016. *Diagnosing large Gulf Stream meanders in the South Atlantic Bight using adjoint sensitivity analysis*. Presented at 2016 Ocean Sci. Meet., New Orleans, LA, Feb. 21–26

Zhu X-H, Kaneko A, Saitoa T, Gohda N. 2001. Kuroshio stream path variation and its associated velocity structures south of Shikoku, Japan. *Geophys. Res. Lett.* 28:4615–18